JACS
JOURNAL OF THE AMERICAN CHEMICAL SOCIETY
pubs.acs.org/JACS

Article

Designing Quantum Spaces of Higher Dimensionality from a Tetranuclear Erbium-Based Single-Molecule Magnet

Angelica P. Orlova, Maximilian G. Bernbeck, and Jeffrey D. Rinehart*

Cite This: J. Am. Chem. Soc. 2024, 146, 23417−23425

Read Online

ACCESS | Metrics & More | Article Recommendations | Supporting Information

ABSTRACT: The spin relaxation of an Er^{3+} tetranuclear single-molecule magnet, $[\mathbf{Er(hdcCOT)I}]_4$, (hdcCOT = hexahydrodicyclopentacyclooctatetraenide dianion), is modeled as a near-tetrahedral arrangement of Ising-type spins. Combining evidence from single-crystal X-ray diffraction, magnetometry, and computational techniques, the slow spin relaxation is interpreted as a consequence of symmetry restrictions imposed on quantum tunneling within the cluster core. The union of spin and spatial symmetries describe a ground state spin−spin coupled manifold wherein 16 eigenvectors generate the 3D quantum spin-space described by the vertices of a rhombic dodecahedron. Analysis of the experimental findings in this context reveals a correlation between the magnetic transitions and edges connecting cubic and octahedral subsets of the eigenspace convex hull. Additionally, the model is shown to map to a theoretically proposed quantum Cayley network, indicating an underexplored synergy between mathematical descriptions of molecular spin interactions and quantum computing configuration spaces.

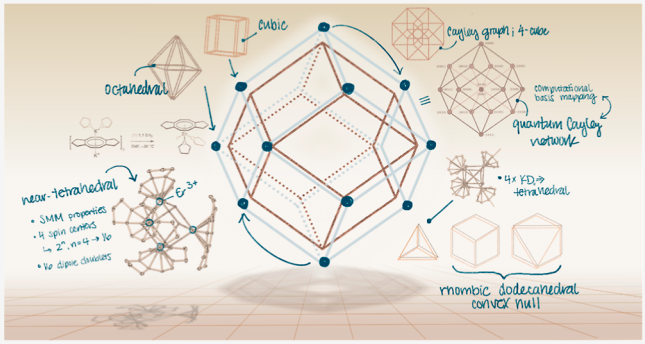

INTRODUCTION

Many research efforts in molecular magnetism are pivoting toward exploring and understanding behaviors of molecular magnets in the context of quantum information science, primarily focusing on quantum computation upon molecular qubits.[1−4] A recent National Academies[5] report describes the necessity of chemists to focus on design, synthesis, measurement, and control of molecular quantum systems, prioritizing addressing and controlling multiple electron spins in molecular systems. To realize molecular versatility and scalability in applications such as quantum computing, simulation, and sensing, current mainstays of chemical intuition that rely on symmetry, charge, and bonding must be adapted to the presence of complex electron spin interactions. Recognizing this, molecular magnetism researchers have sought better control over how the choice of magnetic center and coupling methodology[6] determines the interplay between local (1-site) and global (many-site) responses.[7−10] The search to uncover more fundamental spin-structure−property relationships has led to a growing literature of transition metal,[11−16] lanthanide, and mixed-metal systems[17−25] placed into multispin architectures of clusters,[26,27] chains,[28,29] or extended frameworks.[30−34] The majority of multinuclear (4 or more centers) lanthanide cluster research has focused on dysprosium ions bridged with oxygen,[26,35−39] as dysprosium's propensity toward an axially anisotropic ground state allows for straightforward characterization of SMM (single-molecule magnet) behaviors.[7] We set out to utilize similar energetic perturbative design principles for erbium,[8] trapping it in an highly anisotropic ground state environment through crystal-field effects. However, design of a lanthanide-based cluster[26] SMM via coupling mononuclear SMMs rarely improves upon or even retains the slow relaxation dynamics of the solitary ion, often due to mixing of crystal field states via intraion coupling. To maximize the mapping of single-ion bases onto the coupled cluster interaction, we minimized the energy perturbation by reducing orbital-based exchange interactions, instead relying on a dipole-coupling of the highly anisotropic spins. To further reduce the free-parameter space, a cluster was synthesized with spatial orientation of the Ising axes that approximates the four 3-fold rotation axes of a tetrahedron: $[\mathbf{Er(hdcCOT)I}]_4$, (hdcCOT = hexahydrodicyclopentacyclooctatetraenide dianion).

To address the complexity of this system, we impose symmetry restrictions on the magnetic dipole−dipole portion of the Hamiltonian through crystallographic relationships between individual Er^{3+} centers.[40−43] In such systems, the eigenstates of the total angular momentum can be engineered

Received: May 14, 2024
Revised: July 31, 2024
Accepted: August 1, 2024
Published: August 6, 2024

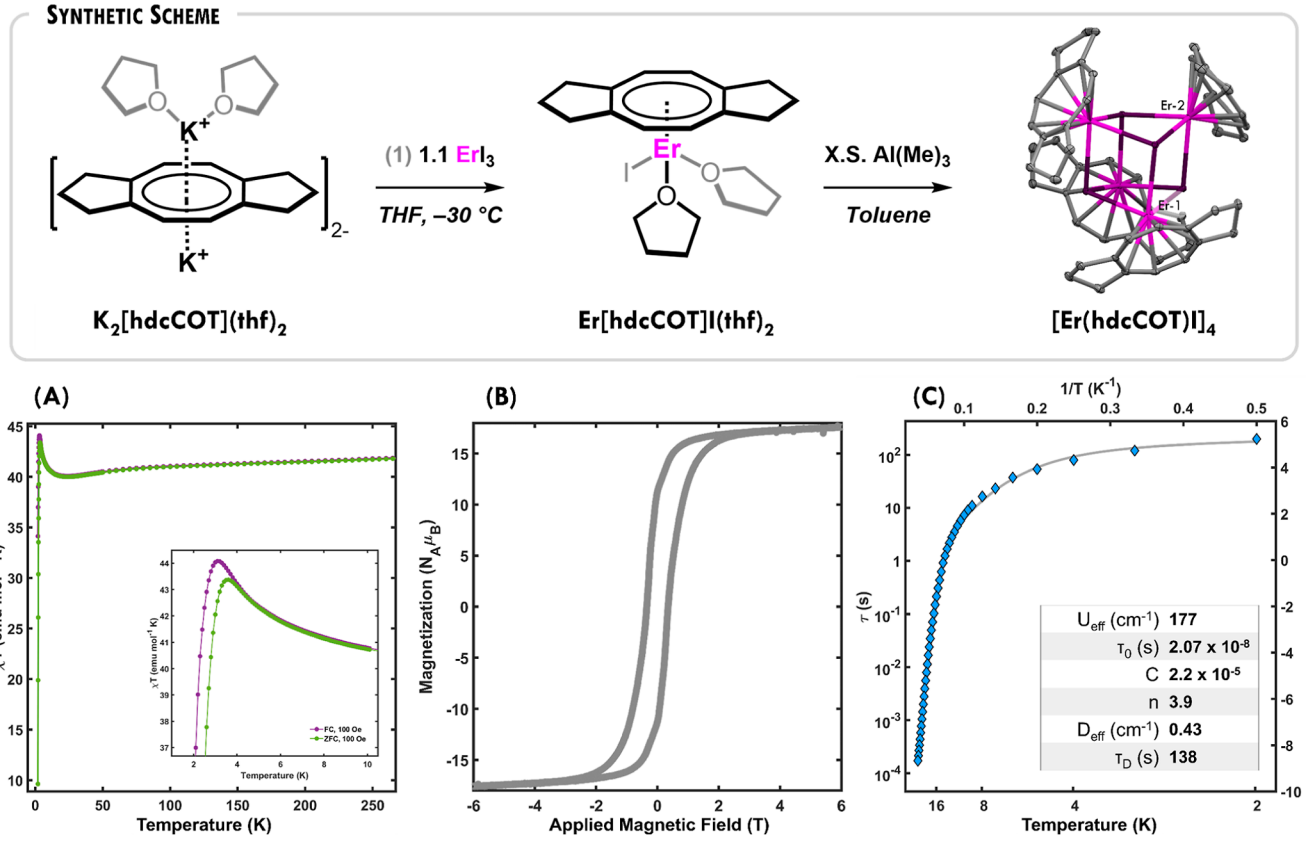

Figure 1. Synthetic scheme and X-ray single-crystal structure of $[\mathbf{Er(hdcCOT)I}]_4$. Ellipsoids in structures represent carbon (gray), iodine (purple), and erbium (pink). Two unique erbium ions within the structure are labeled as Er-1 and Er-2. Hydrogen atoms are omitted for clarity. Magnetic data for $[\mathbf{Er(hdcCOT)I}]_4$: (A) thermal magnetic susceptibility between 2−300 K, collected in FC (purple) and ZFC (green) modes under an applied field of 100 Oe, (B) isothermal magnetization at T = 2 K, 60 Oe/s sweep rate, (C) Arrhenius plots of relaxation times versus temperature (blue diamonds; error bars are within markers for upper and lower error limits of τ values). Gray line is a fit to a multiterm relaxation model (eq S1) with inset table depicting fit parameters.

to be highly predictable, controllable by external fields, and resistant to random field fluctuations. Curiously, the Er^{3+} ion has been incorporated into numerous molecular clusters,[37,44−54] displays high moment and anisotropy,[55−57] yet slow magnetization dynamics are observed in only one instance, and only under induced field.[58] Inspired by pyrochlore structures well-known for spin-ice behavior,[59] theoretical tetrahedral qubit design[60] predicting minimal decoherence, a four-dimensional proposed quantum network with perfect spin transfer,[61] and the potential to implement Ising-type Hamiltonians for quantum computation,[62] we hypothesized that a tetranuclear, tetrahedral molecular analogue would be an interesting subject of study. As such, we present an investigation into the first tetranuclear erbium cluster to exhibit slow magnetic relaxation and SMM behavior, $[\mathbf{Er(hdcCOT)I}]_4$, and offer insights into the computationally derived, dipole-coupled spin states responsible for its magnetic characteristics.

RESULTS & DISCUSSION: SYNTHESIS & MAGNETISM

Synthesis of tetranuclear $[\mathbf{Er(hdcCOT)I}]_4$ proceeds through the addition of K_2[hdcCOT](thf)$_2$ to a suspension of ErI_3 in cold THF in a rigorously air-free environment. This procedure generates the monomeric, Lewis-base adduct, Er[hdcCOT]I-(thf)$_2$ as pink-orange crystals. Subsequently, well-dried crystals of the monomer are dissolved in hot toluene and reacted with excess tetramethylaluminum ($Al(Me)_3$) to abstract THF and form the tetranuclear $[\mathbf{Er(hdcCOT)I}]_4$ as red-orange crystals (Figure 1, synthetic scheme). Single-crystal X-ray diffraction analysis shows that $[\mathbf{Er(hdcCOT)I}]_4$ crystallizes in space group $C2/c$, with two unique erbium ions within the structure. The full structure is composed of four bridging iodide ions connecting four erbium centers situated 4.3645(6)−4.8670(5) Å apart. The Er-hdcCOT units are oriented in a near-tetrahedral environment with respect to the cluster center (τ_4 = 0.94, where τ_4 = 1 is an ideal tetrahedron).[63−65] These units generate the highly anisotropic ground states of each erbium ion, with anisotropy axes directed through each of the hdcCOT centroids. Befitting our previously introduced intuitive model of analysis of anisotropy vectors for such systems,[40] and further corroborated by computational findings in the following section, we are able to see the first spin-structure relationship in this compound: tetrahedral crystallographic arrangement of Er-hdcCOT units generates a tetrahedral spin-space of uncoupled ground Kramers doublets on each erbium ion.

To understand the implications of such a spin-space relationship, we collected static and dynamic data on finely ground microcrystalline samples in an MPMS3 SQUID magnetometer (Supporting Information, Section 4). Susceptibility data were collected in field-cooled (FC) and zero-field-cooled (ZFC) modes under an applied field of 100 Oe between 2 and 300 K and plotted as the susceptibility-

https://doi.org/10.1021/jacs.4c06600
J. Am. Chem. Soc. 2024, 146, 23417−23425

temperature product ($\chi_M T$) vs temperature (Figure 1A). Both curves depict a dramatic rise in thermal susceptibility as temperature increases from 2 K, reaching maxima at 3.1 and 3.5 K, respectively, followed by a steep decrease at higher temperatures, indicative of ferromagnetic coupling interactions operant at these temperatures. Divergence between the FC and ZFC curves at temperatures below 4.4 K indicates magnetic blocking on the time scale of the measurement. By the superparamagnetic blocking definition of $T(\tau = 100\ \text{s})$, the blocking temperature is ~3 K. Around 25 K, both curves begin to slope upward, gradually increasing to a room temperature $\chi_M T$ value of 41.79 emu mol^{-1} K. The compound presents open hysteresis at $T = 2$ K, up to temperatures of ~10 K, saturates near 18 $N_A\mu_B$, and has a coercive field of $H_c = 3500$ Oe (0.35 T; Figure 1B).

A combination of standard AC susceptibility and extended frequency space techniques[32,40,66,67] were utilized to investigate dynamic magnetic behavior. These data are summarized as curves of the natural log of relaxation times versus inverse temperature in order to emphasize the connection to, and deviation from, Arrhenius behavior (Figure 1C). Using a standard phenomenological model, the data is fit to a combination of basic mechanisms: Orbach, Raman, and dipolar (eq S1; dipolar term introduced in prior works[32,40]). At higher temperatures, the relaxation dynamics are consistent with typical SMM Arrhenius behavior, with relaxation through thermal excitation, following the Orbach mechanism. The extracted experimental barrier, $U_{eff} = 177$ cm^{-1}, is in range with the high-temperature dynamics of other Er-COT compounds and derivatives,[8,32,40−42,66,68−75] and outperforms its monomeric counterpart[66] (reported $U_{eff} = 147$ cm^{-1}).

In the context of $[\mathbf{Er(hdcCOT)I}]_4$, the dipolar term encompasses the weakly temperature dependent processes occurring within the ground spin manifold over the temperature range of 2−7 K. In this temperature regime, magnetic relaxation dynamics will be most influenced by small energetic perturbations arising from dipolar coupling interactions between the ground Kramers doublets of each spin center (KD_0, $M_J = \pm 15/2$), and will give rise to 2^n dipole-coupled states, where n is the number of spin centers. Within this context, this small perturbation amounts to a fit $D_{eff} = 0.43$ cm^{-1}. The dipolar attempt time ($\tau_D = 138$ s) and nearly thermal independent behavior are consistent with symmetry restrictions on transitions in a closely spaced manifold of states. Intrigued by the geometric manifestation of the isolated spin spaces, we sought more quantitative corroboration from a computational and theoretical study.

RESULTS & DISCUSSION: COMPUTATIONAL INVESTIGATION

To facilitate our computational study, we took an energetically perturbative approach with respect to the electronic structure of the cluster. First, we utilized CASSCF methods with Single_Aniso, RASSI, RASSCF, and SEWARD modules of OpenMolcas[76−78] to gain insight into the spin−orbit coupling present at the single-ion level within each spin center. Then, we utilized the Poly_Aniso module of OpenMolcas to investigate the spin−spin interactions within the cluster and the emergent dipole-coupled quantum space. These calculations were completed on a set of compounds (Supporting Information, Section 6) to understand the complex spin structure of the cluster and the consequences of symmetry restrictions on the wave function, with the main focus of this work being on two analogues: crystallographic near-tetrahedral $[\mathbf{Er(hdcCOT)I}]_4$, ($\tau_4 = 0.94$) and **Er-T_d**, an idealized model cluster, $[ErCOTI]_4$, with T_d symmetry imposed on the Er−I core using the Largent−Polik−Schmidt algorithm[79,80] ($\tau_4 = 1$; Figure 2; Supporting Information, Section 6).

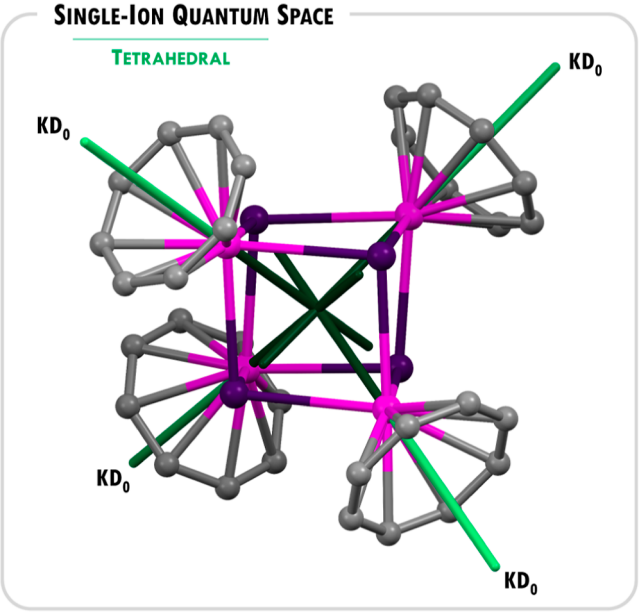

Figure 2. Computationally derived tetrahedral single-ion quantum space of **Er-T_d** with anisotropy axes arising from each spin center's ground Kramers doublet (KD) represented by green lines.

Single-ion calculations were completed on crystallographic coordinates of each erbium center in $[\mathbf{Er(hdcCOT)I}]_4$ and **Er-T_d** and describe the single-ion energy surface composed of Kramers doublets (KDs) of each magnetic ion. Computations show that single-ion energetics are comparable between crystallographic and idealized structures, with highly anisotropic ($g_z = 17.96$, $g_{x,y} = 0.00$), nearly pure $M_J = \pm 15/2$ ground states (KD_0), and $M_J = \pm 13/2$ first excited states (KD_1), separated by ~85 cm^{-1} (vide infra; Supporting Information, Section 6). As expected, and seen in prior compounds, the main anisotropy axes of the ground Kramers doublets (KD_0) of each spin center lie along the Er-COT vector (Figure 2, shown for **Er-T_d** and depicted with green lines). It would be expected that this single-ion electronic profile would be operational at higher temperatures. Interestingly, the experimentally derived barrier ($U_{eff} = 177$ cm^{-1}) is over twice the energy of the first available excited state, and approaches, but does not reach, the second excited state ($KD_2 = 244$ cm^{-1}). This is likely due to a high degree of mixing between KD_2 and KD_3, which encompass $M_J = \pm 1/2$ and $\pm 11/2$ states with ~50% purity. In the idealized tetrahedral cluster, the purity of these states increases substantially (up to 92%), but KD_2 becomes a primarily $M_J = \pm 1/2$ state, making it highly susceptible to facilitate relaxation, even when coupled.

At lower temperatures, transitions between ground and excited KDs become less thermally accessible, and relaxation dynamics are governed by transitions within intramolecularly coupled ground KDs of each magnetic center.[40] To provide insight into this low-temperature relaxation behavior, we generated a phenomenological model of dipole−dipole exchange between the four highly anisotropic, Ising-type,

https://doi.org/10.1021/jacs.4c06600
J. Am. Chem. Soc. 2024, 146, 23417−23425

ground KDs (M_J = ± 15/2) of each magnetic center in the cluster(s) through the Poly_Aniso module of OpenMolcas. The outputs of these calculations provide the dipole-coupled energy manifolds of $[\mathbf{Er(hdcCOT)I}]_4$ and **Er-T_d**, their eigenvalues, and projections in space. Both compound symmetries yield manifolds composed of 16 eigenstates, eight doublets (calculated as pseudospin, $\tilde{S}$ = 1/2, due to the highly axial single-ion states), situated between 0.0 and 4.7 cm^{-1} and referred to as dipole doublets (DD_{0-7}; Table 1). As

Table 1. Computationally Derived Parameters of Dipole-Coupled Quantum Spaces of Idealized Er-T_d and Crystallographic $[Er(hdcCOT)I]_4$.

	Er-T_d		$[Er(hdcCOT)I]_4$	
DD_n, n =	energy (cm^{-1})	eigenvalue	energy (cm^{-1})	eigenvalue
0	0.00	±20.98	0.00	±19.45
1	0.01	±20.67	0.08	±20.11
2	0.02	±20.58	0.52	±22.52
3	1.17	±18.12	1.30	±17.45
4	1.17	±18.08	1.30	±17.45
5	1.18	±17.85	1.36	±18.46
6	1.19	±17.81	1.36	±18.46
7	4.69	±0.23	4.72	±0.80

hypothesized, further degeneracies and interrelationships between states are evident for both the crystallographic and idealized cluster, with **Er-T_d** most clearly elucidating symmetry-induced aspects of the spin structure. The first three multiplets (DD_{0-2}) approach a 6-fold degeneracy. States $DD_{3,4}$ and $DD_{5,6}$ are each 4-fold degenerate, generating two sets of quartets at nearly identical energies. State DD_7 is unique in that its eigenvalues are both nearly zero, indicating an antisymmetrization of all four constituent states.

Intrigued by these initial findings, we sought further indications for how the observed degeneracies could be contextualized in terms of spin and crystallographic symmetry. Our interpretation centers on a geometric analysis based on **Er-T_d**, in which we project eigenvectors of each multiplet from the center of the cluster, scaled by eigenvalue, and generate a three-dimensional visualization of the dipole-coupled magnetic energy surface representing the available quantum space within the low temperature range (Figure 3A). Figure 3A depicts the local magnetic axis of each dipole doublet and highlights the aforementioned degeneracies in three-dimensional space. The convex hull of the available quantum space forms the rhombic dodecahedron, a Catalan solid.[81] Within this, are three subspaces composed of an octahedron, a cube, and a set of points at the origin. States DD_{0-2} are situated orthogonally with respect to each other and take on the configuration of an octahedron (orange, Figure 3A), following their energetic degeneracies. States DD_{3-6} each project through the center of one of the four COT-rings, generating a cube (cyan, Figure 3A), highly reminiscent of the ground KDs. State DD_7 projects almost perfectly onto the origin of our geometric representation (magenta, Figure 3A).

To further discuss transition probabilities within this context, the coordinate system is fixed along the main magnetic axis, aligned with DD_0. The appropriate vector components of each state are projected onto the main magnetic axis (represented with purple dashed arrows, Figure 3B), upholding both the degeneracy and energy of each state. This process retains DD_0 as the ground state and main axis of

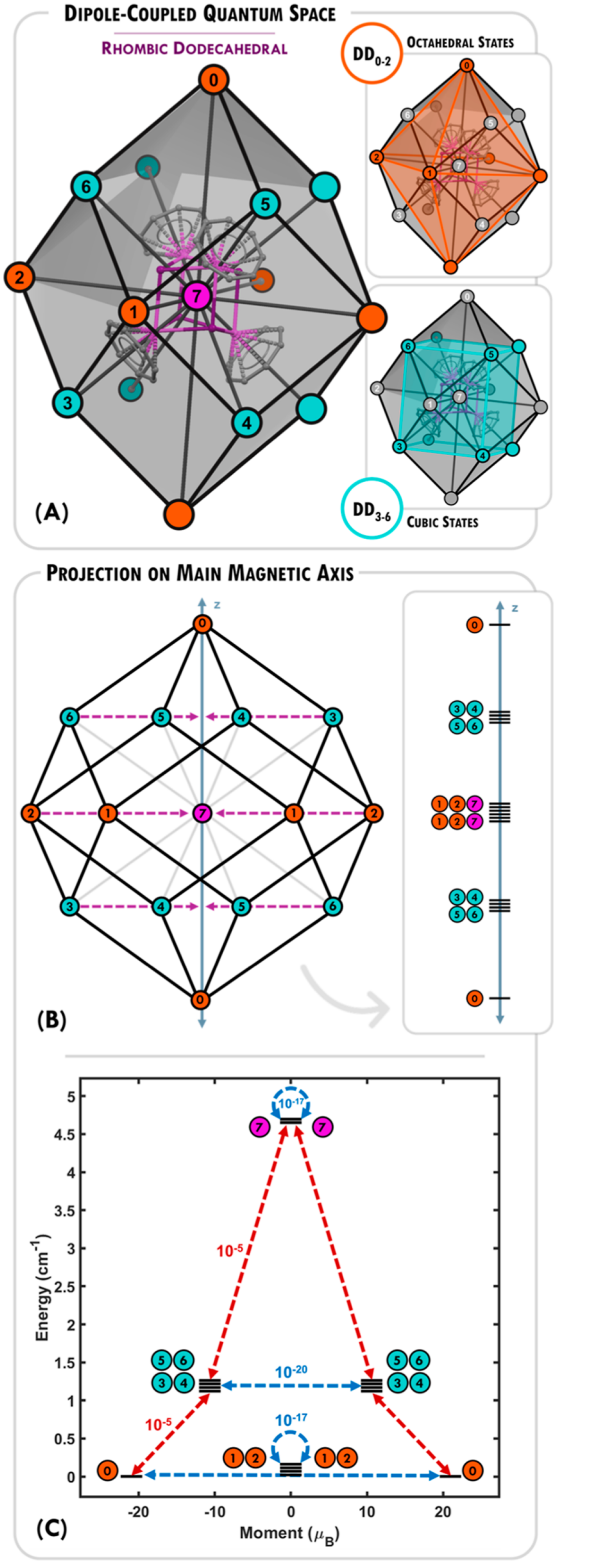

Figure 3. Computationally derived quantum space of **Er-T_d**. (A) Rhombic dodecahedral dipole-coupled quantum space composed of 8 dipole doublets (DDs), labeled numerically. Color corresponds to octahedral (orange) and cubic (cyan) subspaces, as discussed in the text. (B) Simplified representation of (A) depicting projection of states onto the main magnetic z-axis, to generate (C) dipole-coupled energy manifold of states and transition probabilities between them, depicted with as arrows with most (red) and least (blue) probable transitions.

https://doi.org/10.1021/jacs.4c06600
J. Am. Chem. Soc. 2024, 146, 23417−23425

anisotropy, while fully mixing the projections of its degenerate counterparts, DD_1 and DD_2. States DD_{3-6} have partial projections and so retain a scaled version of their cubic representation. This is more clearly evidenced in a familiar energy manifold depicted in Figure 3C, where each DD is organized by its respective energy and moment. The most(least) likely transition probabilities between states are depicted with red(blue) arrows, relating to transition matrix elements connecting eigenstates through a Zeeman perturbation.[82]

Within this idealized model, it is possible to clearly see the impact of symmetry and geometry of the quantum space and begin to relate and rationalize experimentally derived data. The experimental findings at low temperatures coincide with our theoretical predictions and computational modeling; DD_0 is the ferromagnetically coupled exchange state responsible for the ZFC/FC and hysteretic behavior seen experimentally within the low-temperature regime. Its 2-fold degeneracy arises from the nature of anisotropy, which aligns individual spins, creating an energetic equivalence between the "all-in" and "all-out" configurations. In this context, these are quantized by a total pseudospin of $\tilde{S} = \pm 2$.

The probabilities of transitions follow magnetic dipole−dipole selections rules ($\Delta S = \pm 1$) and are equivalent to a single step on one of the edges connecting to DD_0 on the rhombic dodecahedron. This is equivalent to a single spin-flip and is closely related to the concept of Hamming distance[83] from information theory. The fully ferromagnetically coupled ground state (DD_0, $\tilde{S} = \pm 2$) is most likely to transition to one of the cubic states (DD_{3-6}, $\tilde{S} = \pm 1$), each of which is representative of a "one-in, three-out" (or vice versa) spin configuration. It is unlikely to transition to DD_1 or DD_2 ($\tilde{S} = 0$), which allows it to maintain its large anisotropy. As expected, quantum tunnelling of magnetization (QTM) in the dipole-coupled ground states is greatly suppressed (10^{-17} vs 10^{-5} in KD_0) and is similarly suppressed within the cubic states ($\sim 10^{-20}$, Figure 3C). There is no direct pathway involving the smallest distance (one edge) between states on either side of the barrier, and QTM becomes a four-step spin-flip process strongly impacted by dipole coupling present among spins.

From fitting our experimental data, the predicted dipolar energy splitting was determined to be $D_{eff} = 0.43$ cm^{-1}, whereas the calculated dipolar barrier is $\Delta E(DD_0, DD_7) = 4.7$ cm^{-1}, indicating that the highest energy state, DD_7, is unlikely to be involved to an appreciable degree. It is further unlikely that the dipolar barrier is composed of DD_2 ($E = 0.52$ cm^{-1}; Supporting Information Figure S10) as calculated for crystallographic $[\mathbf{Er(hdcCOT)I}]_4$, as this transition would be disallowed by dipolar selection rules, which is further confirmed through calculated matrix probabilities. Following the analysis of the idealized tetrahedral compound, $\mathbf{Er}$-$\boldsymbol{T}_\mathbf{d}$, it appears most likely that the dipolar barrier is composed of the cubic states ($E \sim 1$ cm^{-1}), access to which are allowed by selection rules, and which are within the order of magnitude of the experimentally derived dipolar barrier.

Stimulated by discussion within the field of molecular magnetism toward its applicability to quantum computing, we set out to map a computational basis onto the dipole-coupled quantum space of our tetranuclear compound. To discuss this, we introduce a simple representation of the binary basis in ket-form where the spin at each site is represented by a "0" or "1" (Figure 4). In this depiction, the "all-in" state is represented by $|0000\rangle$ and the "all-out" by $|1111\rangle$, corresponding to DD_0. In this context, traversing between states across one edge is directly related to a unit Hamming distance and the equivalence of one spin-flip per step. Furthermore, the computational basis mapped onto our molecular system becomes representative of a quantum Cayley network,[61] proposed by Facer and co-workers, claimed to be adjustable to perfectly route quantum information between nodes (in our molecular system, these correspond to DD states). The depiction from their work shows an identical configuration of states (nodes) and mapped computational basis, however the two center states are separated, as the quantum Cayley network maps onto a four-dimensional hypercube instead of a three-dimensional rhombic dodecahedron, as in our molecular system.

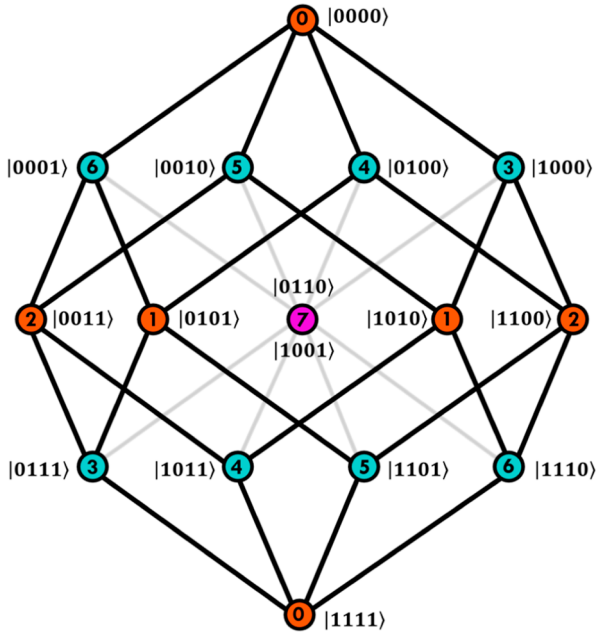

Figure 4. Binary computational basis in ket-representations mapped onto the dipole-coupled quantum space. Numerically ordered circles in orange, cyan, and magenta correspond to dipole doublets, as discussed in the text.

Curiously, the rhombic dodecahedron is a vertex-first parallel-projection of a four-dimensional hypercube into three-dimensional space.[84] We thus hypothesize that the dipole-coupled quantum spaces of $\mathbf{Er}$-$\boldsymbol{T}_\mathbf{d}$ and $[\mathbf{Er(hdcCOT)I}]_4$ may generalize through models that are constructed and manipulated in a higher-dimensional space with projection onto a lower dimensional measurement space only for comparison with experiment. Such models may aid us in rationalizing the superimposed center states (magenta, Figure 4), as well as time-reversal symmetry upon this surface. Investigations to understand and mathematically depict this are underway. Furthermore, we hypothesize that this system could be implemented as a molecular manifestation of a quantum Cayley network, wherein particular cubic states could be accessed with an appropriate application of field. The example we presented depicts an application of field along the z-axis of the molecule, however, due to its crystallographic and emergent quantum space symmetries, applications of field in x- or y-directions could stimulate DD_1 or DD_2 to act as the corresponding ground states. The projections of cubic states could remain analogous to the example presented prior but would project different sets of states onto the two sides of the

https://doi.org/10.1021/jacs.4c06600
J. Am. Chem. Soc. 2024, 146, 23417−23425

dipole barrier. Further investigations to test the propensity of this system as an accessible quantum network are ongoing.

CONCLUSION

In this work we use a geometric approach for discussing the spin structure of a lanthanide cluster, incorporating elements of spin and spatial symmetry to facilitate connection between synthesis, measurement, theory, and computation into a unified hypothesis-driven model of spin architecture design. Our analysis reveals that $[\mathbf{Er(hdcCOT)I}]_4$ has SMM functionality driven by near-tetrahedral symmetry. Computational analysis further shows that this tetrahedral space manifests into a 16-eigenstate dipole-coupled quantum space with a rhombic dodecahedral convex hull composed of octahedral and cubic subspaces. We show that despite vanishingly small energy barriers to relaxation, the additional restrictions on the spin symmetry inhibit QTM, and enforce spin paths that respect magnetic dipole−dipole selection rules. A thermal barrier (U_{eff} = 177 cm^{-1}), well in excess of KD_1, and low-temperature relaxation time of 138 s are strong indicators that $[\mathbf{Er(hdcCOT)I}]_4$ is an SMM because of spin-symmetry restrictions on the Hamiltonian, not purely electrostatic restrictions. Furthermore, we've shown that it is possible to map a computational binary basis onto this system that uses synthetic design and symmetry to leverage the advantages of molecules to design quantum interactions bypassing the standard qubit-by-qubit approach. From these results, we envision the opportunity to further expand upon principles for multinuclear magnetic architectures using the precision and predictability of the dipolar interaction to bring the fundamental goal of designing functional quantum spaces closer to reality.

ASSOCIATED CONTENT

Supporting Information

The Supporting Information is available free of charge at https://pubs.acs.org/doi/10.1021/jacs.4c06600.

Preparative details, sample characterization, physical and computational details for all compounds, equation S1, Figures S1−S10, tables S1−S6 (PDF)

Accession Codes

CCDC 2311633−2311635 contain the supplementary crystallographic data for this paper. These data can be obtained free of charge via www.ccdc.cam.ac.uk/data_request/cif, or by emailing data_request@ccdc.cam.ac.uk, or by contacting The Cambridge Crystallographic Data Centre, 12 Union Road, Cambridge CB2 1EZ, UK; fax: +44 1223 336033.

AUTHOR INFORMATION

Corresponding Author

Jeffrey D. Rinehart − *Department of Chemistry and Biochemistry, University of California, San Diego, La Jolla, California 92093, United States;* orcid.org/0000-0002-5478-1995; Email: jrinehart@ucsd.edu

Authors

Angelica P. Orlova − *Department of Chemistry and Biochemistry, University of California, San Diego, La Jolla, California 92093, United States;* orcid.org/0000-0002-2446-1384

Maximilian G. Bernbeck − *Department of Chemistry and Biochemistry, University of California, San Diego, La Jolla, California 92093, United States;* Present Address: M.G.B. School of Chemistry and Biochemistry, Georgia Institute of Technology, Atlanta, Georgia 30,332, United States; orcid.org/0000-0001-6329-5860

Complete contact information is available at: https://pubs.acs.org/10.1021/jacs.4c06600

Notes

The authors declare no competing financial interest.

ACKNOWLEDGMENTS

This research was funded through the National Science Foundation Division of Chemistry #2154830. We are thankful to the W. M. Keck Laboratory for Integrated Biology for time on their supercomputer; the UCSD Crystallography Facility, especially Drs. Milan Gembicky and Jake Bailey; to the Figueroa Group, especially Krista P. Balto, for the use of their FT-IR instrument; A.P.O. is grateful to Dr. Doran Spencer for sustained eye functionality. A.P.O. is grateful to Dr. Jules M. Moutet and J.D.R. is grateful to Professor Srinivasan S. Iyengar for useful and stimulating discussions.

REFERENCES

(1) Gaita-Ariño, A.; Luis, F.; Hill, S.; Coronado, E. Molecular spins for quantum computation. *Nat. Chem.* **2019**, *11* (4), 301−309.

(2) Wasielewski, M. R.; Forbes, M. D. E.; Frank, N. L.; Kowalski, K.; Scholes, G. D.; Yuen-Zhou, J.; Baldo, M. A.; Freedman, D. E.; Goldsmith, R. H.; Goodson, T.; Kirk, M. L.; McCusker, J. K.; Ogilvie, J. P.; Shultz, D. A.; Stoll, S.; Whaley, K. B. Exploiting chemistry and molecular systems for quantum information science. *Nat. Rev. Chem* **2020**, *4* (9), 490−504.

(3) Stewart, R.; Canaj, A. B.; Liu, S.; Regincós Martí, E.; Celmina, A.; Nichol, G.; Cheng, H.-P.; Murrie, M.; Hill, S. Engineering Clock Transitions in Molecular Lanthanide Complexes. *J. Am. Chem. Soc.* **2024**, *146* (16), 11083−11094.

(4) Smith, P. W.; Hrubý, J.; Evans, W. J.; Hill, S.; Minasian, S. G. Identification of an X-Band Clock Transition in Cp′3Pr- Enabled by a 4f25d1 Configuration. *J. Am. Chem. Soc.* **2024**, *146* (9), 5781−5785.

(5) National Academies of Sciences, E.; Medicine *Advancing Chemistry and Quantum Information Science: An Assessment of Research Opportunities at the Interface of Chemistry and Quantum Information Science in the United States*; The National Academies Press: Washington, DC, 2023.

(6) Chen, Y. C.; Tong, M. L. Single-molecule magnets beyond a single lanthanide ion: the art of coupling. *Chem. Sci.* **2022**, *13* (30), 8716−8726.

(7) Rinehart, J. D.; Long, J. R. Exploiting single-ion anisotropy in the design of f-element single-molecule magnets. *Chem. Sci.* **2011**, *2* (11), 2078−2085.

(8) Hilgar, J. D.; Bernbeck, M. G.; Flores, B. S.; Rinehart, J. D. Metal-ligand pair anisotropy in a series of mononuclear Er-COT complexes. *Chem. Sci.* **2018**, *9* (36), 7204−7209.

(9) Wäckerlin, C.; Cahlík, A.; Goikoetxea, J.; Stetsovych, O.; Medvedeva, D.; Redondo, J.; Svec, M.; Delley, B.; Ondráček, M.; Pinar, A.; Blanco-Rey, M.; Kolorenc, J.; Arnau, A.; Jelínek, P. Role of the Magnetic Anisotropy in Atomic- Spin Sensing of 1 D Molecular Chains. *ACS Nano* **2022**, *16* (10), 16402−16413.

(10) Briganti, M.; Lucaccini, E.; Chelazzi, L.; Ciattini, S.; Sorace, L.; Sessoli, R.; Totti, F.; Perfetti, M. Magnetic Anisotropy Trends along a Full 4f-Series: The f^{n+7} Effect. *J. Am. Chem. Soc.* **2021**, *143* (21), 8108−8115.

(11) Gatteschi, D. Physical techniques for the investigation of molecular magnetic clusters. *J. Phys. Chem. B* **2000**, *104* (42), 9780−9787.

(12) Li, D. F.; Parkin, S.; Wang, G. B.; Yee, G. T.; Clerac, R.; Wernsdorfer, W.; Holmes, S. M. An *S* = 6 Cyanide-Bridged

Octanuclear $Fe^{III}_4Ni^{II}_4$ Complex that Exhibits Slow Relaxation of the Magnetization. *J. Am. Chem. Soc.* **2006**, *128* (13), 4214−4215.
(13) Li, D. F.; Parkin, S.; Wang, G. B.; Yee, G. T.; Holmes, S. M. Early metal di- and tricyanometalates: Useful building blocks for constructing magnetic clusters. *Inorg. Chem.* **2006**, *45* (7), 2773−2775.
(14) Maniaki, D.; Pilichos, E.; Perlepes, S. P. Coordination Clusters of 3d-Metals That Behave as Single-Molecule Magnets (SMMs): Synthetic Routes and Strategies. *Front Chem.* **2018**, *6*, 1−28.
(15) Mertes, K. M.; Suzuki, Y.; Sarachik, M. P.; Myasoedov, Y.; Shtrikman, H.; Zeldov, E.; Rumberger, E. M.; Hendrickson, D. N.; Christou, G. Mn12-acetate: a prototypical single molecule magnet. *Solid State Commun.* **2003**, *127* (2), 131−139.
(16) Boskovic, C.; Brechin, E. K.; Streib, W. E.; Folting, K.; Bollinger, J. C.; Hendrickson, D. N.; Christou, G. Single-Molecule Magnets: A New Family of Mn_{12} Clusters of Formula $[Mn_{12}O_8X_4(O_2CPh)_8L_6]$. *J. Am. Chem. Soc.* **2002**, *124* (14), 3725−3736.
(17) Han, H. T.; Li, X. L.; Zhu, X. F.; Zhang, G. S.; Hang, X. X.; Tang, J. K.; Liao, W. P. Single-Molecule Magnetic Behavior in a Calix[8]arene-Capped Heterometallic $\{Dy^{III}_4Co^{II}_4\}$ Square-Antiprismatic Cluster. *Eur. J. Inorg. Chem.* **2017**, *2017* (41), 4879−4883.
(18) Li, M. Y.; Lan, Y. H.; Ako, A. M.; Wernsdorfer, W.; Anson, C. E.; Buth, G.; Powell, A. K.; Wang, Z. M.; Gao, S. A Family of 3d-4f Octa-Nuclear $[Mn^{III}_4Ln^{III}_4]$ Wheels (Ln = Sm, Gd, Tb, Dy, Ho, Er, and Y): Synthesis, Structure, and Magnetism. *Inorg. Chem.* **2010**, *49* (24), 11587−11594.
(19) Mereacre, V.; Akhtar, M. N.; Lan, Y. H.; Ako, A. M.; Clérac, R.; Anson, C. E.; Powell, A. K. Structures and magnetic properties of MnIII4LnIII4 aggregates with a "square-in-square" topology. *Dalton Trans.* **2010**, *39* (20), 4918−4927.
(20) Perfetti, M.; Rinck, J.; Cucinotta, G.; Anson, C. E.; Gong, X. J.; Ungur, L.; Chibotaru, L.; Boulon, M. E.; Powell, A. K.; Sessoli, R. Single Crystal Investigations Unravel the Magnetic Anisotropy of the "Square-In Square" CrDy SMM Coordination Cluster. *Front Chem.* **2019**, *7:6*, 1−8.
(21) Moreno Pineda, E.; Heesing, C.; Tuna, F.; Zheng, Y. Z.; McInnes, E. J. L.; Schnack, J.; Winpenny, R. E. P. Copper Lanthanide Phosphonate Cages: Highly Symmetric $\{Cu_3Ln_9P_6\}$ and $\{Cu_6Ln_6P_6\}$ Clusters with C_{3v} and D_{3h} Symmetry. *Inorg. Chem.* **2015**, *54* (13), 6331−6337.
(22) Vignesh, K. R.; Langley, S. K.; Swain, A.; Moubaraki, B.; Damjanovic, M.; Wernsdorfer, W.; Rajaraman, G.; Murray, K. S. Slow Magnetic Relaxation and Single-Molecule Toroidal Behaviour in a Family of Heptanuclear $\{Cr^{III}Ln^{III}_6\}$ (Ln=Tb, Ho, Er) Complexes. *Angew. Chem. Int. Edit* **2018**, *57* (3), 779−784.
(23) Xiang, H.; Lu, W. G.; Jiang, L.; Zhang, W. X.; Lan, Y. H. A Family of Double Cubanes $\{Cr^{III}_2Ln^{III}_4O_6\}$ (Ln = Tb, Ho, Er, Yb, Y) Based on Sulfate: Single-Molecule Magnet Behavior in the Terbium and Erbium Analogues. *Eur. J. Inorg. Chem.* **2016**, *2016* (6), 907−912.
(24) Zheng, Y. Z.; Evangelisti, M.; Tuna, F.; Winpenny, R. E. P. Co-Ln Mixed-Metal Phosphonate Grids and Cages as Molecular Magnetic Refrigerants. *J. Am. Chem. Soc.* **2012**, *134* (2), 1057−1065.
(25) Stati, D.; van Leusen, J.; Ahmed, N.; Kravtsov, V. C.; Kögerler, P.; Baca, S. G. A {CoIII2DyIII4} Single-Molecule Magnet with an Expanded Core Structure. *Cryst. Growth Des.* **2023**, *23* (1), 395−402.
(26) Han, T.; Ding, Y. S.; Zheng, Y. Z. Lanthanide Clusters Toward Single-Molecule Magnets. *Struct. Bonding.* **2016**, *173*, 209−314.
(27) Ungur, L.; Lin, S. Y.; Tang, J. K.; Chibotaru, L. F. Single-molecule toroics in Ising-type lanthanide molecular clusters. *Chem. Soc. Rev.* **2014**, *43* (20), 6894−6905.
(28) Pedersen, K. S.; Vindigni, A.; Sessoli, R.; Coulon, C.; Clérac, R. Single-Chain Magnets. In *Molecular Magnetic Materials*; John Wiley & Sons, Ltd, 2017; pp 131−159.
(29) Huang, G.; Daiguebonne, C.; Calvez, G.; Suffren, Y.; Guillou, O.; Guizouarn, T.; Le Guennic, B.; Cador, O.; Bernot, K. Strong Magnetic Coupling and Single-Molecule-Magnet Behavior in Lanthanide-TEMPO Radical Chains. *Inorg. Chem.* **2018**, *57* (17), 11044−11057.
(30) Huang, G.; Fernandez-Garcia, G.; Badiane, I.; Camarra, M.; Freslon, S.; Guillou, O.; Daiguebonne, C.; Totti, F.; Cador, O.; Guizouarn, T.; Le Guennic, B.; Bernot, K. Magnetic Slow Relaxation in a Metal-Organic Framework Made of Chains of Ferromagnetically Coupled Single-Molecule Magnets. *Chem.—Eur. J.* **2018**, *24* (27), 6983−6991.
(31) Journaux, Y.; Ferrando-Soria, J.; Pardo, E.; Ruiz-Garcia, R.; Julve, M.; Lloret, F.; Cano, J.; Li, Y. L.; Lisnard, L.; Yu, P.; Stumpf, H.; Pereira, C. L. M. Design of Magnetic Coordination Polymers Built from Polyoxalamide Ligands: A Thirty Year Story. *Eur. J. Inorg. Chem.* **2018**, *2018* (3−4), 228−247.
(32) Orlova, A. P.; Varley, M. S.; Bernbeck, M. G.; Kirkpatrick, K. M.; Bunting, P. C.; Gembicky, M.; Rinehart, J. D. Molecular Network Approach to Anisotropic Ising Lattices: Parsing Magnetization Dynamics in Er^{3+} Systems with 0−3-Dimensional Spin Interactivity. *J. Am. Chem. Soc.* **2023**, *145* (40), 22265−22275.
(33) Yang, Z. X.; Gong, F.; Lin, D. M.; Huo, Y. Recent advances in polyoxometalate-based single-molecule magnets. *Coord. Chem. Rev.* **2023**, *492*, 215205.
(34) Manna, F.; Oggianu, M.; Avarvari, N.; Mercuri, M. L. Lanthanide-Based Metal-Organic Frameworks with Single-Molecule Magnet Properties. *Magnetochemistry* **2023**, *9* (7), 190.
(35) Lin, P. H.; Korobkov, I.; Wernsdorfer, W.; Ungur, L.; Chibotaru, L. F.; Murugesu, M. A Rare μ_4-O Centred Dy_4 Tetrahedron with Coordination-Induced Local Chirality and Single-Molecule Magnet Behaviour. *Eur. J. Inorg. Chem.* **2011**, *2011* (10), 1535−1539.
(36) Anwar, M. U.; Thompson, L. K.; Dawe, L. N.; Habib, F.; Murugesu, M. Predictable self-assembled [2 × 2] Ln(III)(4) square grids (Ln = Dy,Tb)-SMM behaviour in a new lanthanide cluster motif. *Chem. Commun.* **2012**, *48* (38), 4576−4578.
(37) Chandrasekhar, V.; Das, S.; Dey, A.; Hossain, S.; Sutter, J. P. Tetranuclear Lanthanide (III) Complexes Containing Dimeric Subunits: Single-Molecule Magnet Behavior for the Dy-4 Analogue. *Inorg. Chem.* **2013**, *52* (20), 11956−11965.
(38) Guo, P. H.; Liu, J. L.; Zhang, Z. M.; Ungur, L.; Chibotaru, L. F.; Leng, J. D.; Guo, F. S.; Tong, M. L. The First {Dy-4} Single-Molecule Magnet with a Toroidal Magnetic Moment in the Ground State. *Inorg. Chem.* **2012**, *51* (3), 1233−1235.
(39) Wang, B.; Wei, C. Y. Structures, fluorescent properties and single-molecule-magnet behavior of two Ln4 (LnIII = Tb and Dy) clusters. *J. Mol. Struct.* **2020**, *1216*, 128241.
(40) Orlova, A. P.; Hilgar, J. D.; Bernbeck, M. G.; Gembicky, M.; Rinehart, J. D. Intuitive Control of Low-Energy Magnetic Excitations via Directed Dipolar Interactions in a Series of Er(III)-Based Complexes. *J. Am. Chem. Soc.* **2022**, *144* (25), 11316−11325.
(41) Hilgar, J. D.; Bernbeck, M. G.; Rinehart, J. D. Million-fold Relaxation Time Enhancement across a Series of Phosphino-Supported Erbium Single-Molecule Magnets. *J. Am. Chem. Soc.* **2019**, *141* (5), 1913−1917.
(42) Bernbeck, M. G.; Hilgar, J. D.; Rinehart, J. D. Probing axial anisotropy in dinuclear alkoxide-bridged Er-COT single-molecule magnets. *Polyhedron* **2020**, *175*, 114206.
(43) Bernbeck, M. G.; Orlova, A. P.; Hilgar, J. D.; Gembicky, M.; Ozerov, M.; Rinehart, J. D. Dipolar Coupling as a Mechanism for Fine Control of Magnetic States in ErCOT-Alkyl Molecular Magnets. *J. Am. Chem. Soc.* **2024**, *146* (11), 7243−7256.
(44) Abbas, G.; Lan, Y. H.; Kostakis, G. E.; Wernsdorfer, W.; Anson, C. E.; Powell, A. K. Series of Isostructural Planar Lanthanide Complexes $[Ln^{III}_4(\mu_3\text{-}OH)_2(mdeaH)_2(piv)_8]$ with Single Molecule Magnet Behavior for the Dy_4 Analogue. *Inorg. Chem.* **2010**, *49* (17), 8067−8072.
(45) Biswas, S.; Das, S.; Gupta, T.; Singh, S. K.; Pissas, M.; Rajaraman, G.; Chandrasekhar, V. Observation of Slow Relaxation and Single-Molecule Toroidal Behavior in a Family of Butterfly-Shaped Ln_4 Complexes. *Chem.—Eur. J.* **2016**, *22* (51), 18532−18550.
(46) Blagg, R. J.; Ungur, L.; Tuna, F.; Speak, J.; Comar, P.; Collison, D.; Wernsdorfer, W.; McInnes, E. J. L.; Chibotaru, L. F.; Winpenny,

https://doi.org/10.1021/jacs.4c06600
J. Am. Chem. Soc. 2024, 146, 23417−23425

R. E. P. Magnetic relaxation pathways in lanthanide single-molecule magnets. *Nat. Chem.* **2013**, *5* (8), 673−678.
(47) Chen, H. M.; Wang, W. M.; Li, X. Q.; Chu, X. Y.; Nie, Y. Y.; Liu, Z.; Huang, S. X.; Shen, H. Y.; Cui, J. Z.; Gao, H. L. Luminescence and magnetocaloric effect of Ln_4 clusters (Ln = Eu, Gd, Tb, Er) bridged by CO_3^{2-} deriving from the spontaneous fixation of carbon dioxide in the atmosphere. *Inorg. Chem. Front.* **2018**, *5* (2), 394−402.
(48) Gao, H. L.; Huang, S. X.; Zhou, X. P.; Liu, Z.; Cui, J. Z. Magnetic properties and structure of tetranuclear lanthanide complexes based on 8-hydroxylquinoline Schiff base derivative and *β*-diketone coligand. *Dalton Trans.* **2018**, *47* (10), 3503−3511.
(49) Gao, H. L.; Zhou, X. P.; Bi, Y. X.; Shen, H. Y.; Wang, W. M.; Wang, N. N.; Chang, Y. X.; Zhang, R. X.; Cui, J. Z. A Dy4 single-molecule magnet and its Gd(iii), Tb(iii), Ho(iii), and Er(iii) analogues encapsulated by an 8-hydroxyquinoline Schiff base derivative and *β*-diketonate coligand. *Dalton Trans.* **2017**, *46* (14), 4669−4677.
(50) Li, X. L.; Li, F. C.; Zhang, X. L.; Liu, Y. F.; Wang, A. L.; Tian, J. F.; Xiao, H. P. Synthesis, crystal structures and magnetic properties of two tetranuclear lanthanide-hydroxo cubane clusters. *Synth. Met.* **2015**, *209*, 220−224.
(51) Lin, S. Y.; Sun, B. D.; Xu, Z. K. Syntheses, structures and magnetic properties of chiral lanthanide tetrahedral clusters supported by symmetrical amidate ligands. *Inorg. Chim. Acta* **2017**, *464*, 119−124.
(52) Luan, F.; Yan, P. F.; Zhu, J.; Liu, T. Q.; Zou, X.; Li, G. M. A salen-type Dy_4 single-molecule magnet with an enhanced energy barrier and its analogues. *Dalton Trans.* **2015**, *44* (9), 4046−4053.
(53) Pajerowski, D. M.; Li, Q.; Hyun, J.; Dennis, C. L.; Phelan, D.; Yan, P. F.; Chen, P.; Li, G. M. Chloride-bridged, defect-dicubane $\{Ln_4\}$ core clusters: syntheses, crystal structures and magnetic properties. *Dalton Trans.* **2014**, *43* (31), 11973−11980.
(54) Zhang, H. F.; Zhang, J.; Li, Y. H.; Qin, Y. R.; Chen, Y. M.; Liu, W.; Gao, D. D.; Li, W. A series of tetranuclear $[Ln_4]$ clusters with defect-dicubane cores including a Dy_4 single-molecule magnet. *J. Coord. Chem.* **2015**, *68* (16), 2798−2809.
(55) Feng, W. X.; Zhang, Y.; Zhang, Z.; Lü, X.; Liu, H.; Shi, G. X.; Zou, D.; Song, J. R.; Fan, D. D.; Wong, W. K.; Jones, R. A. Anion-Induced Self-Assembly of Luminescent and Magnetic Homoleptic Cyclic Tetranuclear $Ln_4(Salen)_4$ and $Ln_4(Salen)_2$ Complexes (Ln = Nd, Yb, Er, or Gd). *Inorg. Chem.* **2012**, *51* (21), 11377−11386.
(56) Sukhikh, T. S.; Bashirov, D. A.; Kuratieva, N. V.; Smolentsev, A. I.; Bogomyakov, A. S.; Burilov, V. A.; Mustafina, A. R.; Zibarev, A. V.; Konchenko, S. N. New NIR-emissive tetranuclear Er(III) complexes with 4-hydroxo-2,1,3-benzothiadiazolate and dibenzoylmethanide ligands: synthesis and characterization. *Dalton Trans.* **2015**, *44* (12), 5727−5734.
(57) Zhao, J. Y.; Yang, C.; Bian, X. Y.; Qiu, J.; Ren, S. Y.; Fang, M. A tetranuclear Er(III)-based cluster with bifunctional properties: Efficient conversion of CO2 and slow magnetic relaxation behavior. *Inorg. Chim. Acta* **2023**, *556*, 121560.
(58) Koo, B. H.; Lim, K. S.; Ryu, D. W.; Lee, W. R.; Koh, E. K.; Hong, C. S. A unique tetranuclear ErIII4 cluster exhibiting field-induced single-molecule magnetism. *Chem. Commun.* **2012**, *48* (19), 2519−2521.
(59) Bramwell, S. T.; Gingras, M. J. P. Spin Ice State in Frustrated Magnetic Pyrochlore Materials. *Science* **2001**, *294* (5546), 1495−1501.
(60) Feigel'man, M. V.; Ioffe, L. B.; Geshkenbein, V. B.; Dayal, P.; Blatter, G. Superconducting tetrahedral quantum bits. *Phys. Rev. Lett.* **2004**, *92* (9), 098301.
(61) Facer, C.; Twamley, J.; Cresser, J. Quantum Cayley networks of the hypercube. *Phys. Rev. A* **2008**, *77* (1), 012334.
(62) Saha, D.; Iyengar, S. S.; Richerme, P.; Smith, J. M.; Sabry, A. Mapping Quantum Chemical Dynamics Problems to Spin-Lattice Simulators. *J. Chem. Theory Comput.* **2021**, *17* (11), 6713−6732.
(63) Rosiak, D.; Okuniewski, A.; Chojnacki, J. Novel complexes possessing Hg-(Cl, Br, I)···OC halogen bonding and unusual Hg2S2(Br/I)4 kernel. The usefulness of *τ*4′ structural parameter. *Polyhedron* **2018**, *146*, 35−41.
(64) Okuniewski, A.; Rosiak, D.; Chojnacki, J.; Becker, B. Coordination polymers and molecular structures among complexes of mercury(II) halides with selected 1-benzoylthioureas. *Polyhedron* **2015**, *90*, 47−57.
(65) Yang, L.; Powell, D. R.; Houser, R. P. Structural variation in copper(i) complexes with pyridylmethylamide ligands: structural analysis with a new four-coordinate geometry index, *τ*4. *Dalton Trans.* **2007**, No. 9, 955−964.
(66) Hilgar, J. D.; Butts, A. K.; Rinehart, J. D. A method for extending AC susceptometry to long-timescale magnetic relaxation. *Phys. Chem. Chem. Phys.* **2019**, *21* (40), 22302−22307.
(67) Blackmore, W. J. A.; Gransbury, G. K.; Evans, P.; Kragskow, J. G. C.; Mills, D. P.; Chilton, N. F. Characterisation of magnetic relaxation on extremely long timescales. *Phys. Chem. Chem. Phys.* **2023**, *25* (25), 16735−16744.
(68) Hilgar, J. D.; Flores, B. S.; Rinehart, J. D. Ferromagnetic coupling in a chloride-bridged erbium single-molecule magnet. *Chem. Commun.* **2017**, *53* (53), 7322−7324.
(69) Xue, T. J.; Ding, Y. S.; Reta, D.; Chen, Q. W.; Zhu, X. F.; Zheng, Z. P. Closely Related Organometallic Er(III) Single-Molecule Magnets with Sizably Different Relaxation Times of Quantum Tunneling of Magnetization. *Cryst. Growth Des.* **2023**, *23* (1), 565−573.
(70) Chen, S.-M.; Xiong, J.; Zhang, Y.-Q.; Yuan, Q.; Wang, B.-W.; Gao, S. A soft phosphorus atom to "harden" an erbium(iii) single-ion magnet. *Chem. Sci.* **2018**, *9* (38), 7540−7545.
(71) Meng, Y.-S.; Wang, C.-H.; Zhang, Y.-Q.; Leng, X.-B.; Wang, B.-W.; Chen, Y.-F.; Gao, S. (Boratabenzene)(cyclooctatetraenyl) lanthanide complexes: a new type of organometallic single-ion magnet. *Inorg. Chem. Front.* **2016**, *3* (6), 828−835.
(72) Ungur, L.; Le Roy, J. J.; Korobkov, I.; Murugesu, M.; Chibotaru, L. F. Fine-tuning the Local Symmetry to Attain Record Blocking Temperature and Magnetic Remanence in a Single-Ion Magnet**. *Angew. Chem. Int. Edit* **2014**, *53* (17), 4413−4417.
(73) Le Roy, J. J.; Ungur, L.; Korobkov, I.; Chibotaru, L. F.; Murugesu, M. Coupling Strategies to Enhance Single-Molecule Magnet Properties of Erbium-Cyclooctatetraenyl Complexes. *J. Am. Chem. Soc.* **2014**, *136* (22), 8003−8010.
(74) Le Roy, J. J.; Korobkov, I.; Murugesu, M. A sandwich complex with axial symmetry for harnessing the anisotropy in a prolate erbium(iii) ion. *Chem. Commun.* **2014**, *50* (13), 1602−1604.
(75) Meihaus, K. R.; Long, J. R. Magnetic Blocking at 10 K and a Dipolar-Mediated Avalanche in Salts of the Bis(*η*8-cyclooctatetraenide) Complex [Er(COT)2]-. *J. Am. Chem. Soc.* **2013**, *135* (47), 17952−17957.
(76) Aquilante, F.; Autschbach, J.; Baiardi, A.; Battaglia, S.; Borin, V. A.; Chibotaru, L. F.; Conti, I.; De Vico, L.; Delcey, M.; Fdez Galván, I.; Ferré, N.; Freitag, L.; Garavelli, M.; Gong, X.; Knecht, S.; Larsson, E. D.; Lindh, R.; Lundberg, M.; Malmqvist, P. Å.; Nenov, A.; Norell, J.; Odelius, M.; Olivucci, M.; Pedersen, T. B.; Pedraza-González, L.; Phung, Q. M.; Pierloot, K.; Reiher, M.; Schapiro, I.; Segarra-Martí, J.; Segatta, F.; Seijo, L.; Sen, S.; Sergentu, D.-C.; Stein, C. J.; Ungur, L.; Vacher, M.; Valentini, A.; Veryazov, V. Modern quantum chemistry with [Open]Molcas. *J. Chem. Phys.* **2020**, *152* (21), 214117.
(77) Fdez Galván, I.; Vacher, M.; Alavi, A.; Angeli, C.; Aquilante, F.; Autschbach, J.; Bao, J. J.; Bokarev, S. I.; Bogdanov, N. A.; Carlson, R. K.; Chibotaru, L. F.; Creutzberg, J.; Dattani, N.; Delcey, M. G.; Dong, S. S.; Dreuw, A.; Freitag, L.; Frutos, L. M.; Gagliardi, L.; Gendron, F.; Giussani, A.; González, L.; Grell, G.; Guo, M.; Hoyer, C. E.; Johansson, M.; Keller, S.; Knecht, S.; Kovačević, G.; Källman, E.; Li Manni, G.; Lundberg, M.; Ma, Y.; Mai, S.; Malhado, J. P.; Malmqvist, P. Å.; Marquetand, P.; Mewes, S. A.; Norell, J.; Olivucci, M.; Oppel, M.; Phung, Q. M.; Pierloot, K.; Plasser, F.; Reiher, M.; Sand, A. M.; Schapiro, I.; Sharma, P.; Stein, C. J.; Sørensen, L. K.; Truhlar, D. G.; Ugandi, M.; Ungur, L.; Valentini, A.; Vancoillie, S.; Veryazov, V.; Weser, O.; Wesołowski, T. A.; Widmark, P.-O.; Wouters, S.; Zech, A.;

https://doi.org/10.1021/jacs.4c06600
J. Am. Chem. Soc. 2024, 146, 23417−23425

Zobel, J. P.; Lindh, R. OpenMolcas: From Source Code to Insight. *J. Chem. Theory Comput.* **2019**, *15* (11), 5925−5964.
(78) Li Manni, G.; Fdez Galván, I.; Alavi, A.; Aleotti, F.; Aquilante, F.; Autschbach, J.; Avagliano, D.; Baiardi, A.; Bao, J. J.; Battaglia, S.; Birnoschi, L.; Blanco-González, A.; Bokarev, S. I.; Broer, R.; Cacciari, R.; Calio, P. B.; Carlson, R. K.; Carvalho Couto, R.; Cerdán, L.; Chibotaru, L. F.; Chilton, N. F.; Church, J. R.; Conti, I.; Coriani, S.; Cuéllar-Zuquin, J.; Daoud, R. E.; Dattani, N.; Decleva, P.; de Graaf, C.; Delcey, M. G.; De Vico, L.; Dobrautz, W.; Dong, S. S.; Feng, R. L.; Ferré, N.; FilatovGulak, M.; Gagliardi, L.; Garavelli, M.; González, L.; Guan, Y. F.; Guo, M. Y.; Hennefarth, M. R.; Hermes, M. R.; Hoyer, C. E.; Huix-Rotllant, M.; Jaiswal, V. K.; Kaiser, A.; Kaliakin, D. S.; Khamesian, M.; King, D. S.; Kochetov, V.; Krosnicki, M.; Kumaar, A. A.; Larsson, E. D.; Lehtola, S.; Lepetit, M. B.; Lischka, H.; López Ríos, P.; Lundberg, M.; Ma, D. X.; Mai, S.; Marquetand, P.; Merritt, I. C. D.; Montorsi, F.; Mörchen, M.; Nenov, A.; Nguyen, V. H. A.; Nishimoto, Y.; Oakley, M. S.; Olivucci, M.; Oppel, M.; Padula, D.; Pandharkar, R.; Phung, Q. M.; Plasser, F.; Raggi, G.; Rebolini, E.; Reiher, M.; Rivalta, I.; Roca-Sanjuán, D.; Romig, T.; Safari, A. A.; Sánchez-Mansilla, A.; Sand, A. M.; Schapiro, I.; Scott, T. R.; Segarra-Martí, J.; Segatta, F.; Sergentu, D. C.; Sharma, P.; Shepard, R.; Shu, Y. N.; Staab, J. K.; Straatsma, T. P.; Sorensen, L. K.; Tenorio, B. N. C.; Truhlar, D. G.; Ungur, L.; Vacher, M.; Veryazov, V.; Voß, T. A.; Weser, O.; Wu, D. H.; Yang, X. C.; Yarkony, D.; Zhou, C.; Zobel, J. P.; Lindh, R. The OpenMolcas *Web*: A Community-Driven Approach to Advancing Computational Chemistry. *J. Chem. Theory Comput.* **2023**, *19* (20), 6933−6991.
(79) Largent, R. J.; Polik, W. F.; Schmidt, J. R. Symmetrizer: Algorithmic determination of point groups in nearly symmetric molecules. *J. Comput. Chem.* **2012**, *33* (19), 1637−1642.
(80) Polik, W. F.; Schmidt, J. R. WebMO: Web-based computational chemistry calculations in education and research. *Wires Comput. Mol. Sci.* **2022**, *12* (1), 1−22.
(81) Catalan, E. Mémoire sur la théorie des polyèdres. *J. Ecole Polytechn.* **1865**, *24*, 1−71.
(82) Ungur, L.; Thewissen, M.; Costes, J.-P.; Wernsdorfer, W.; Chibotaru, L. F. Interplay of Strongly Anisotropic Metal Ions in Magnetic Blocking of Complexes. *Inorg. Chem.* **2013**, *52* (11), 6328−6337.
(83) Hamming, R. W. Error Detecting and Error Correcting Codes. *Bell Syst. Tech J.* **1950**, *29* (2), 147−160.
(84) Coxeter, H. S. M.*Regular Polytopes*; Dover Publications, 1973.

https://doi.org/10.1021/jacs.4c06600
J. Am. Chem. Soc. 2024, 146, 23417−23425